2010

VOLUMETRIC GROWTH MODEL OF HUMAN MEDULLOBLASTOMA IN THE NUDE MOUSE CEREBELLUM

Thomas Gavigan
Virginia Commonwealth University

Volumetric Growth Model of Human Medulloblastoma in the Nude Mouse Cerebellum

A thesis submitted in partial fulfillment of the requirements for the degree of Master of Science at Virginia Commonwealth University.

By

Thomas Sanderson Gavigan
B.S., University of North Carolina at Chapel Hill, 2002

Director: William C. Broaddus, M.D., Ph.D.
F. Norton Hord, Jr. Professor
Department of Neurosurgery
Anatomy and Neurobiology

Co-Director: Timothy E. Van Meter, Ph.D.
Assistant Professor
Department of Neurosurgery

Virginia Commonwealth University
Richmond, Virginia
August, 2010

Acknowledgement

So many wonderful individuals have helped me succeed in this endeavor, and I am infinitely grateful for their contributions to this project. Without them, I would not have been able to accomplish my goals for this project. And the learning curve would have been much steeper.

I am grateful for this excellent opportunity provided by my advisor, Dr. William Broaddus. He challenged me to find success and take ownership of this project, and always managed to find time for meetings despite his busy schedule. I wish to thank Dr. Timothy Van Meter, my co-advisor, for his expertise and patience with my technical training and project planning. Further, his intellectual contributions added greatly to this project. I would also like to thank the final member of my committee, Dr. Jack Haar, for his support and constructive guidance.

I wish to thank the other members of the lab, Dr. Nick Pullen, Dr. Helen Fillmore, Archana Chidambaram, MBBS, and Monica Anand, whose personal and professional support motivated me to succeed at my tasks. Their contributions to my project were largely unseen but indispensible, nonetheless. Casual interaction with these individuals made work much more pleasant, and they were an excellent resource for lab work and otherwise.

I cannot thank Dr. Mike Schultz enough for his knowledge and patience with my technical training. His guidance and availability added greatly to this project. I would also like to thank Frank Corwin for the time he dedicated to my MRI work. I wish to extend a thank you to Dr. Jorge Almenara, whose expertise was critical to my project's success.

I am truly grateful to Dr. George Liechnetz, who gave me the opportunity to achieve my goals. He has been integral to my success, and my personal and professional development. Without his support, none of this work was possible. Further, I would like to thank the many faculty members in my department for their unwavering support, intellectual contributions and personal expertise that inspired me to seek excellence in my endeavors, in particular, Dr. John Bigbee and Dr. Randall Merchant.

I also wish to thank Mr. Harold Greenwald in the Graduate School Office, his professionalism and temperament made administrative work a breeze.

Finally, I would like to thank my family and friends for everything that they have contributed during my time on this project, and for all they have done to bring me where I am today. I am truly blessed to have a family that has made every effort to see me succeed. My mother has been a driving force in my life, constantly expecting more from me and encouraging me to achieve my best. My father is the individual I wish to emulate; he is a gifted physician, stoic leader and better father. My sister and brothers have always been supported me, and their companionship has served as a welcome respite from the difficulties of school and life. They have pushed me to be my best, to evaluate every situation and apply what I have learned.

Table of Contents

List of Tables

List of Figures

List of Abbreviations

AKT	Protein kinase B
BSA	Bovine Serum Albumin
CBTRUS	Central Brain Tumor Registry of the United States
CNS	Central Nervous System
CSF	Cerebrospinal Fluid
CT	Computed Tomography
DAOY	Established Medulloblastoma cell line
DKK1	Dickkopf-related protein 1
DMEM	Dulbecco's Modified Eagle Medium
ECL	Chemiluminescent reagent
EGL	External Granular Layer
FBS	Fetal Bovine Serum
Gd-DTP	Gadolinium diethylenetriamine pentaacetic acid
GNP	Granule Neuron Precursors
H&E	Hemotoxylin and eosin
HRR	Homologous recombination
ICP	Intracranial Pressure
IGL	Internal Granular Layer
KCNA1	Potassium voltage-gated channel member 1
LCA	Large Cell Anaplastic Subtype
Lj	Lambda
MB	Medulloblastoma
MBEN	Medulloblastoma with extensive nodularity subtype
MRI	Magnetic Resonance Imaging
NPR3	Natriuretic peptide receptor C
PBS	Phosphate buffer solution
PCL	Purkinje Cell Layer
PCR	Polymerase Chain Reaction
PI3K	Phosphatidylinositol 3-kinases
PNET	Premitive Neuroectodermal Tumor
PTCH1	Patched-1 gene
RIPA	Radio-Immunoprecipitation Assay
RT	Real-Time
SCID	Severe Combined Immunodeficiency
SFRP1	Secreted frizzled-related protein 1
Shh	Sonic Hedgehog
Smo	Smoothened homolog
TPER	Tissue Protein Extraction Reagent
WHO	World Health Organization
Wnt	Wingless

Abstract

VOLUMETRIC GROWTH MODEL OF HUMAN MEDULLOBLASTOMA IN THE NUDE MOUSE CEREBELLUM

By Thomas Sanderson Gavigan, M.S.

A thesis submitted in partial fulfillment of the requirements for the degree of Master of Science at Virginia Commonwealth University.

Virginia Commonwealth University, 2010.

Director: William C. Broaddus, M.D. Ph.D.
F. Norton Hord, Jr. Professor
Department of Neurosurgery

Co-Director: Timothy E. Van Meter, Ph.D.
Associate Professor
Department of Neurosurgery

Medulloblastoma is the most common brain tumor in children, accounting for 10-20% of primary central nervous system (CNS) neoplasms and approximately 40% of all posterior fossa tumors. It is a highly invasive embryonal neuroepithelial tumor that typically arises in the cerebellar vermis and has a tendency to disseminate throughout the CNS early in its course. The molecular mechanisms of the disease largely remain uncharacterized, as the clinical treatment is still associated with mortality and severe side effects. The

development of a clinically relevant in vivo model is important not only to further understand the disease but also to provide a method with which to test novel therapeutics. This study quantified the volumetric growth of a human medulloblastoma (VC312) in the athymic nude mouse cerebellum using Gd-enhanced T1-weighed MRI scans. Additionally, a medulloblastoma flank tumor model was used to explore the in vivo effect of the oral anti-cancer agent that inhibits Akt activation in the phosphoinositide 3-kinase (PI3K) pathway. In the orthotopic intracerebellar tumor model, perifosine significantly increased the survival of treated mice while qualitatively reducing leptomeningeal dissemination. In the flank model, perifosine effectively suppressed the volumetric growth, decreased activation of the AKT pathway and reduced cellular proliferation in treated mice.

Chapter 1

Introduction

Brain Tumors

The brain tumor is for both patients and physicians one of the most dramatic forms of human disease. While primary brain tumors only account for 2% of cancer deaths, their occurrence is responsible for 7% of years of life lost before the age of 70 (Kaye and Laws 1995). An estimated 22,070 new cases of primary malignant brain and central nervous system tumors were diagnosed in the United States in 2009 (12,010 in males and 10,060 in females). This represents approximately 1.5% of all primary malignant cancers diagnosed in the United States in 2009 (CBTRUS, 2009).

A primary brain tumor is an accumulation of abnormal cells that starts within the cranial vault. A brain tumor can arise from the tissue of the brain, around the brain, nerves, or glands. Tumors can destroy normal brain cells via inflammatory response, causing increased intracranial pressure, or by direct cell-to-cell contact (Buckner et al., 2007). Brain tumors are classified by where they appear in the Central Nervous System (CNS), which includes the brain and spinal cord, the kind of tissue that is involved, the cellular aggressiveness or grade, and malignancy (Buckner at el 2007). The WHO classification is a common

neoplasm scaling system that was ratified in 1993 to classify each tumor based on its cell of origin (Kleihues et al 1993).

The difference between normal and neoplastic growth occurs with the disruption of several crucial elements of central nervous system (CNS) development. First, normal cell processes such as modulation of cell proliferation, differentiation and cell death are altered. Second, the alteration of the microenvironment in and around the cell changes important regulatory cues. Thirdly, the combination of these alterations generates a new combination of signals that have an effect on the cells intrinsic biologic activity, leading to the abnormal growth (Kaye and Laws 1995).

The most common malignant brain tumor in children is the medulloblastoma (MB) (CBTRUS, 2009), a highly invasive embryonal neuroepithelial tumor that arises in the cerebellum and tends to disseminate throughout the CNS early in its course (MacDonald, 2010). Unfortunately, one-third of MB tumors remain incurable - while multimodality treatment has improved survival, these interventions nevertheless have several damaging effects in the long run. Novel therapies include small molecule inhibitors such as perifosine, which has proven effective in peripheral cancers. Improved tumor classification will help improve directed treatment. An improved model of the tumor will include assessment of molecular profiles of the MB and estimated growth rates (Gilbertson et al., 2008).

Medulloblastoma

Epidemiology: Infratentorial Primitive Neuroectodermal Tumor

The classification of Primitive Neuroectodermal Tumor or PNET was proposed in 1973 by Hart and Earle. While this distinction was useful in developing clinical protocols to treat a range of CNS embryonal tumors, especially in children, medulloblastomas demonstrate a confounding diversity, unlike other PNETs. For example, the architectural and cytological features of the nodular versus desmoplastic medulloblastoma histologic subtypes are unique. The MB's separation from other PNETs has evolved across editions of the WHO (World Health Organization) classification of CNS tumors (1993, 2000, 2007) and reflects the MB origin and nature. The MB is now recognized as a distinctive tumor defined by its morphologic and genetic attributes (Gilbertson et al, 2008). Recent genetic data out of the Arthur and Sonia Labatt Brain Tumour Research Centre, Toronto, Ontario, Canada further enforces this idea by dividing the tumor into four distinct molecular subtypes (Northcott et al., 2010).

By definition the MB arises in the posterior fossa, specifically in the cerebellum (Rorke et al., 1983). It develops in the vermis and often invades and occupies the fourth ventricle; further invasion can involve the brain stem (Halperin et al., 2005). MB accounts for 13% of childhood primary brain and CNS tumors (CBTRUS 2010), accounting for approximately 540 diagnosed cases a year in the US. The peak age of incidence is 7 years and the tumor is more often seen in boys than girls. The WHO classifies the medulloblastoma as one of five embryonal tumors due to its primitive cellular structure, and grade IV because of its aggressive tendency to metastasize (Kleihues et al., 1993). Approximately 30% of pediatric patients present with cerebrospinal fluid (CSF) metastasis (Fouladi et al., 1999).

Clinical and Laboratory Findings

Symptoms

Medulloblastoma patients most commonly present with a three-month history of headaches, morning vomiting and lethargy. Due to the tumor's classic location in the fourth ventricle, patients may experience clumsiness and problems with simple tasks. These initial symptoms are secondary to increased Intracranial Pressure (ICP). Initial signs of ICP are subtle and difficult to diagnose. School age children often show decreased academic performance and personality changes.

As the tumor increases in size and begins invading the surrounding cerebellum, the characteristic symptoms appear. A particularly common symptom is progressively worsening ataxia mainly in the lower extremities (T. MacDonald et al., 2009). For infants, the symptoms are more difficult to diagnose. Mainly, infants demonstrate difficulty in gazing upward and appear to have a forced downward eye deviation, the "setting-sun sign" (R.J. Packer et al., 1999).

While MB typically disseminates early in the course of the disease, symptoms of the metastases are not characteristic to patient presentation (Halperin EC et al., (2005).

Diagnosis

Most patients with medulloblastoma are diagnosed with a CT scan or MRI. The tumor will appear as a "solid, homogeneous, isodense to hyperdense, contrast-enhancing, midline cerebellar mass" (Zimmerman et al., 1978). The MRI is useful for determining the anatomic origin, extent of the disease and ruling out cerebellar astrocytoma and ependymoma, which appear similar on the CT scan (MacDonald et al., 2009).

Figure 1-1. T1-weighted, Contrast-enhanced MRI of a 4-year-old with medulloblastoma. Note the enhanced mass within the fourth ventricle. Image taken from Polkinghorn, Figure 1 (2007).

Pathology

Found in the cerebellum, the MB is typically a highly cellular, soft, friable tumor composed of cells with deeply basophilic nuclei of variable size and shape, sparsely discernible cytoplasm, and abundant mitoses. With the desmoplastic subtype, the tumors appear lobulated, sharply demarcated and firm, due to reticulin and collagen deposition, when excised surgically (Rosai et al. 2004). MBs show a strong tendency to disseminate through the cerebrospinal pathways and form tumors of variable size along ventricular surfaces, in the subarachnoid space, or along nerve roots. They have been found to grow "en plaque" adjacent to brain or spinal cord (R. Packer et al. 1999). In various cases, Homer-Wright Rosettes, which are ring-like accumulations of tumor cell nuclei around a neuropil-containing or fibrillary core, are present. Varying levels of neuronal and glial differentiation are present, suggesting the cell of origin has the potential for multiple states of differentiation (T. MacDonald et al. 2009).

Molecular biology/ Pathogenesis of Medulloblastomas

Medulloblastoma typically arises in the vermis of the cerebellum during stages of cerebellar development. The cerebellum is the site of a greater density of neurons than the cortex and involves complex signaling pathways during development. A common source of medulloblastoma development is an aberrant signal from the Sonic Hedgehog (Shh) or Wingless (Wnt) pathway. These

signaling molecules are glycoproteins that are secreted from the Purkinje cell layer (PCL) of the cerebellum during cerebellar evolution. In normal development, the Shh or Wnt signal from the Purkinje cells communicates with the granule cells in the external granular layer (EGL) to differentiate and migrate through the PCL to the internal granular layer (IGL) where they form neurons. It has been proposed that medulloblastoma develops when there is an aberrant Shh or Wnt signal from the Purkinie cells, causing the granule cells to divide uncontrollably without proper differentiation and migration. Medulloblastoma is interesting because the mutations cause variable tumor histology with tumor cells that range from completely undifferentiated to extensively nodulated and advanced neuronal differentiation (Fan et al., 2008).

Histology

The medulloblastoma can divided into four different subtypes based on it's histology; Classic, Desmoplastic, Anaplastic and Extensive Nodularity. The classic MB is believed to be Wnt pathway derived and comprises 65% of all diagnoses. The classic histology shows densely packed cells with hyperchromatic nuclei and the cells appear to be mostly undifferentiated (Polkinghorn et al. 2007). Apoptosis is frequent, whereas areas of necrosis are less common (Kleihues et al. 1997).

The desmoplastic subtype is associated with a mutated patched-1 (PTCH1) gene and overactive Shh, making up 25% of all MBs (Polkinghorn et al. 2007). The histology shows characteristic pale islands with abundant reticulin and collagen, reduced cellularity, rarefied fibrillar matrix and increased apoptosis (Rosai et al. 2004).

The anaplastic or large cell MB shows large, round nuclei with prominent nucleoli and large areas of necrosis. This subtype shows considerable cytologic overlap and appears to constitute a unified entity. Usually high mitotic rates, typically abundant apoptotic cellular remains may form "confluent lakes and serpiginous seams" (Rosai et al. 2004). It has been shown that the anaplastic subtype incorporates multiple or an accumulation of mutations, with an association with decreased survival; it makes up only 5% of MBs (Brown HG et al. 2000).

The extensive nodularity subtype (MBEN) appears to be a variation of the desmoplastic subtype with extensive nodularity and advanced neuronal differentiation. This subtype is typified by the linear streaming of rounded, neuron cell bodies, and tumor cell nuclei within amassed cytoplasmic processes (Rosai et al 2004). Defined by the WHO as MB with "intranodular nuclear uniformity on a desmoplastic background" (Giangaspero et al., 2007)., this subtype is found mostly in infants, is associated with a good prognosis and makes up 5% of all MBs (Giangaspero F et al., 1999).

Figure 1-2. Histologic Subtypes of Medulloblastoma. Classic MB with densely packed, hyperchromatic nuclei. Cells appear to be undifferentiated (A), Desmoplastic MB with abundant reticulin and collagen (B), Anaplastic / Large Cell (LCA) MB with large, round nuclei, prominent nucleoli and large areas of necrosis(C), and Extensive Nodularity MB with extensive nodules and advanced neuronal differentiation (D). Images taken from Rosai: Surgical Pathology 9th Edition (2004).

A.

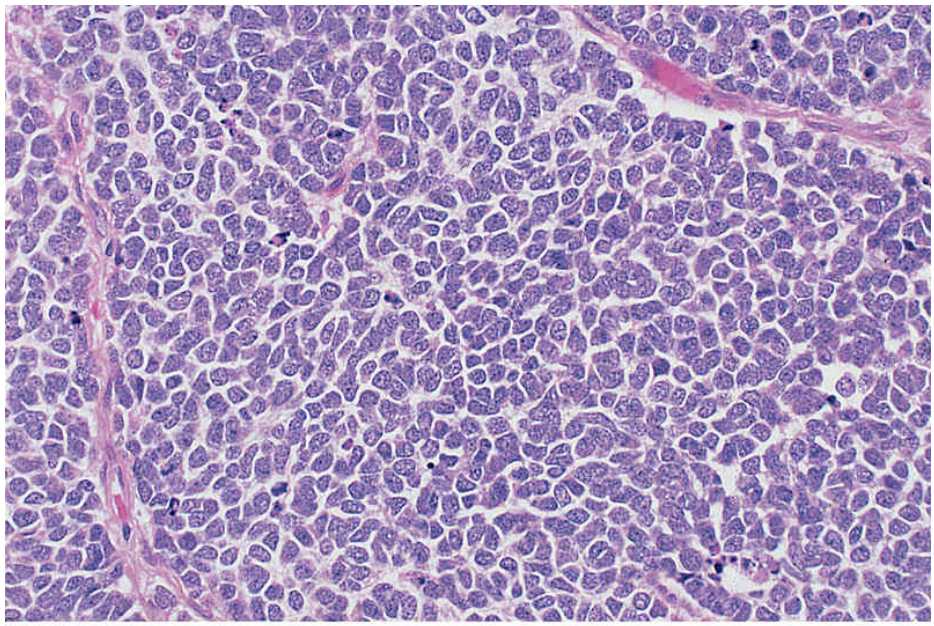

B.

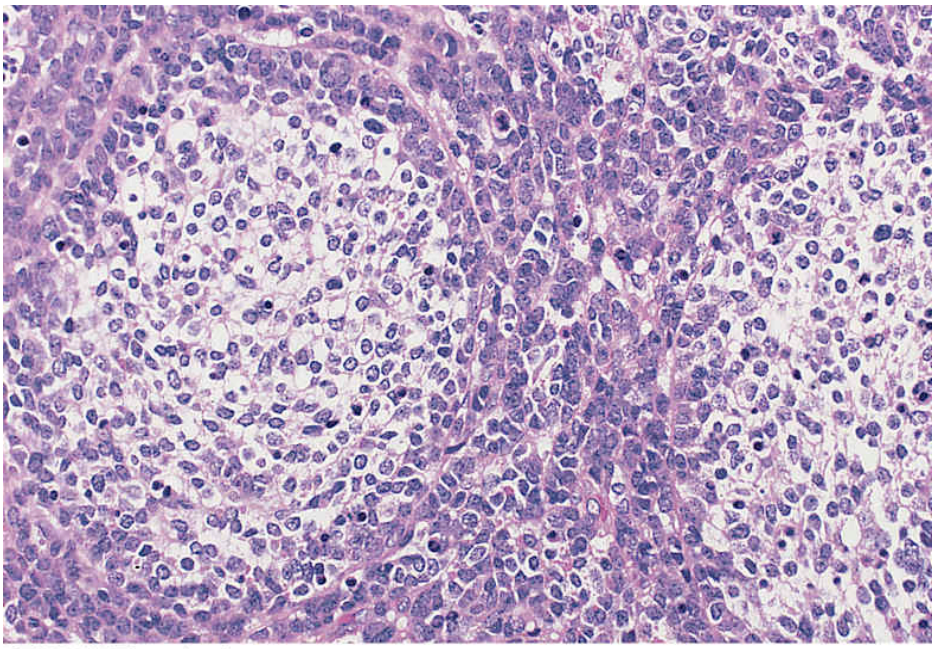

C.

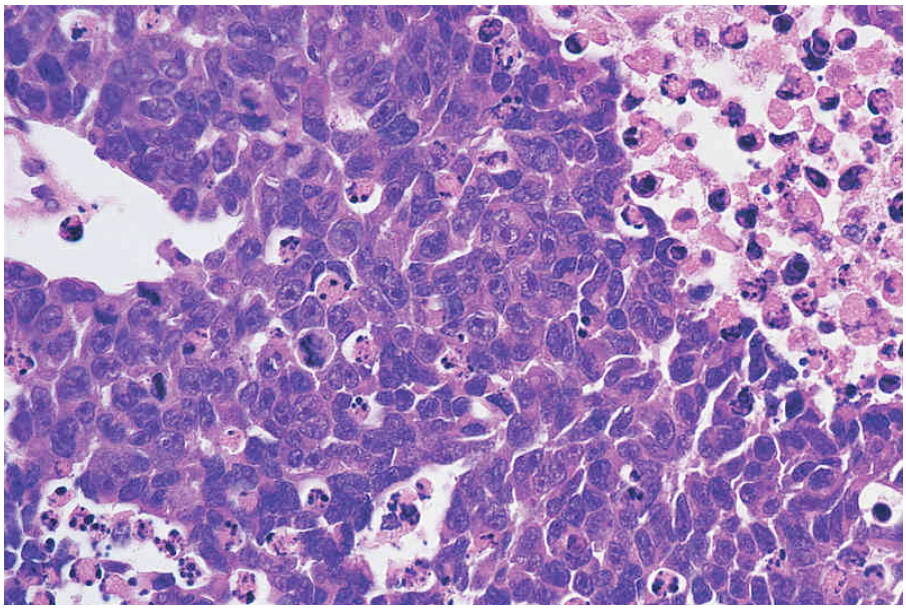

D.

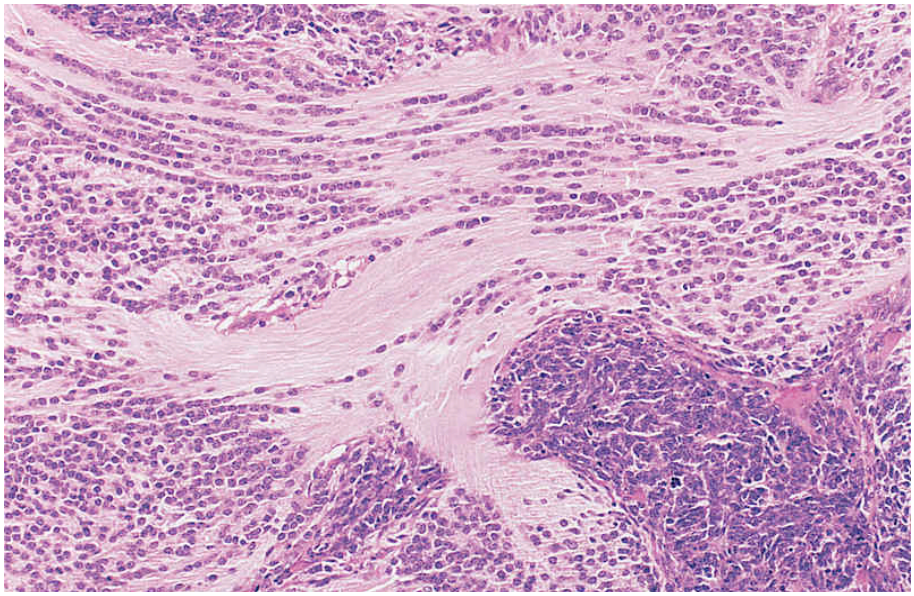

Molecular Subtypes

Recent studies performed by Paul Northcott and colleagues at the University of Toronto Hospital for Sick Children indicate that medulloblastoma has four distinct molecular subtypes. Using Affymetrix and SNP genotyping arrays they identified the following subtypes: WNT, SHH, Group C and Group D. Each subgroup had a 'signature' gene that was over-expressed that was identified by commercial antibodies. The genes and their associated subgroup are: DKK1 (WNT), SFRP1 (SHH), NPR3 (Group C) and KCNA1 (Group D) (Northcott et al. 2010).

Treatment

The current treatment regimen includes surgery, aggressive chemotherapy, and relatively high doses of craniospinal radiation therapy. Despite these therapies, 5-year survival is at best 60% to 80%, and moreover, these therapies affect the developing central nervous system causing memory-, attention-, motor function-, language-, and visuospatial deficits (Ribi et al. 2005).

Models of Medulloblastoma

Clinically relevant animal models are needed for the understanding of tumor biology and testing novel therapies in medulloblastoma. The literature documents many experimental models of MBs, as described below.

In vitro

In vitro studies are commonplace in research laboratories and allow for exploration of tumor cell invasiveness and its causative mechanisms. Ranger et al, used five distinct MB cell lines in 3-D collagen gel assay to assess tumor aggressiveness in vitro. While the three dimensional analysis of the MB cell lines effectively maintains the complex relationships between tumor cells in a 3-D environment, the model lacks the unique in vivo interactions of the CNS.

Transgenic Mice

Current models of MB transgenic mice have problems with failure to generate high tumor incidence and variable latency. A current model developed by Hatton, Villavicencio, Tsuchiya et al.(2008), involves the production of a Smo/Smo homozygous mouse, in which a constitutively active form of the Smoothened gene is expressed under a granule neuron precursor (GNP)-specific promoter. This medulloblastoma model shows increased tumor incidence, predictable tumor latency and displayed a leptomeningeal dissemination of MB cells to the brain and spine. The model appears to recreate the highly aggressive and invasive nature of the human disease. GNPs normally undergo

massive expansion during CNS development and their proliferation is regulated by the Shh and Notch signaling pathways. The Shh binds to the PTCH receptor on GNPs and derepresses the Smoothened receptor, which activates the Shh target transcription. The results of this mouse model producing tumors with multiple features of clinically encountered medulloblastoma suggests that mutations of this pathway are implicated in the formation of medulloblastoma (Hatton, Villavicencio, Tsuchiya et al. 2008). While the transgenic model is a valuable tool for research, it does not incorporate the various types of mutations found in human MB tumors. Further, creating transgenic mice is expensive, is not easily reproducible and does not use human tumor-derived cultured cells. Therefore, the study of human tumors is impossible with this model.

Knock Out Mice

In knock out mice, an endogenous gene is replaced with a gene that does not function correctly. The mouse is said to be homozygous or heterozygous defective depending on whether both or one, respectively, of the homolog genes are defective. This method of engineering mice can be faulty if the target gene plays a role in development. This causes the mice to die before birth or shortly thereafter, which is ineffective for research. A technique for generating conditional knockouts has been created to alleviate this problem by turning off a particular gene after it has played its role in embryogenesis. The use of genetically engineered mice are valuable to researchers because they allow the discovery of which cell signaling pathways play a role in the formation of MB.

While the signaling pathways activated in a mouse tumor can be similar to those activated in the human disease, there will be distinct differences between the human and mouse MB. Therefore, a mouse model of human tumor-derived cells is still necessary.

Flank Tumor Model

While the cerebellum is the "true" environment of the MB, a flank tumor model has a faster course, is more easily observable, and more tightly controlled regarding tumorigenicity and growth parameters. Subcutaneous flank inoculation of athymic nude mice was chosen for this study in addition to orthotopic implantation in the cerebellum (see below), because it models a non permissive growth environment in which tumor cells must appropriately sense and respond to their surroundings to maintain viability, and provides an efficient manner of direct tumor growth observation (Pullen, 2010). Therefore, the effect of therapeutic treatment could be compared against it's effect in mice following intra-cerebellar implantation of tumor cells.

Orthotopic Model of Medulloblastoma in Mouse Cerebellum

The orthotopic tumor models present an amount of complexity superior to classical pathological models. The implantation of tumor cells in their original tissue allows development of tumor comparable to human tumor with production of metastasis and interaction of tumor cells with surrounding tissue. This in situ model can provide a reproducible, reliable and objective method of studying the

effects of therapeutics. Xiumei Zhao recently established that orthotopic xenograft mouse models of MB replicated the key histopathological phenotypes and invasive growth characteristics of the original patient tumors. This group showed that serially passed MB cell lines maintain molecular characteristics for at least three generations, thereby proving that xenograft tumors are molecularly accurate (Zhao et al. 2010). This further demonstrates the necessity of developing a clinically relevant model of the medulloblastoma to examine new therapies that can decrease debilitating therapeutic side effects and treatment failures that plague patients of MB.

We designed experiments using this information with the intent of creating a molecularly accurate, human tumor-derived medulloblastoma model, studying the growth of the disease in the cerebellum, and defining a growth curve for MB to enable evaluation of potential new therapeutics for treatment of the disease.

Therapeutics

Perifosine

AKT, also known as Protein Kinase B, is a regulator of cellular survival pathways aberrantly active in many human cancers including MB, contributing to cellular growth, proliferation and survival (Gills and Dennis, 2009). These characteristics also make AKT an attractive target in cancer therapy and many inhibitors of AKT are being developed. Perifosine is an oral AKT inhibitor

currently being tested in phase 2 clinical trials in peripheral cancers. It is an alkyl-phospholipid, small molecule inhibitor that acts as a competitive inhibitor of AKT-kinases. The in vitro effects of the drug have been studied extensively in our lab by Anil Kumar (Kumar et al., 2009). It was found that Perifosine treatment in vitro led to the rapid induction of cell death in MB cell lines, with marked suppression of phosphorylated AKT in time- and concentration-dependent manners (Kumar et al. 2009). The in vitro studies performed in our lab in combination with the proven effectiveness of perifosine in peripheral cancers made it an ideal candidate for this study.

Chapter 2

Hypothesis and Specific Aims

Rationale: Thorough examination of many models of medulloblastoma has not shown that an existing model can easily reproduce a human tumor-derived othrotopic model of the disease. Tumor volumes provide an objective method of studying the tumor growth and effects of therapeutic agents. The debilitating side effects and treatment failures demand new/improved therapies. We attempted to create a medulloblastoma model in the nude mouse cerebellum that mimics the molecular fidelity, subtype and histology of the human derived tumor. Further, we compared this model to Perifosine-treated mice.

Hypothesis I: Human cultured medulloblastoma tumor cells can be induced to grow in the cerebellum of athymic nude mice to create an orthotopic model.

Specific Aims:

1. Establish effective delivery and placement of tumor inoculum into the cerebellum.
2. Establish a xenograft tumor line with a highly reproducible growth pattern in vivo.
3. Determine the histologic and molecular subtype of medulloblastoma grown in the cerebellum.

Hypothesis II: Tumor volume can be measured accurately using MRI to determine the volumetric growth of the medulloblastoma.

Specific Aims:

1. Objectively determine the volume of the tumor from MRI scan data.
2. Determination of in vivo growth pattern of primary medulloblastoma in mouse cerebellum.

Hypothesis III: Orthotopic model can be used to demonstrate the effectiveness of therapeutics in an in situ model.

Specific Aim:

1. Validate the effective suppression of target signaling molecules and volumetric growth in vivo after Perifosine treatment.

Chapter 3

Methods

All animal experiments were approved by the Committee for the Care and Use of Laboratory Animals at Virginia Commonwealth University. Female athymic nude Fox n1 mice (Harlan, Indianapolis, Indiana) with an average weight of 18 to 22 grams were used for all infusions of medulloblastoma cells.

Stereotactic Infusion

Female athymic nude mice were anesthetized by inhalation administration of 0.3 μL/min isoflurane and maintained in an anesthetized state with 0.2 μL/min isoflurane during the surgery. Lubricating veterinary ointment was applied to the eyes and the animal was placed on a heating pad in a stereotactic frame. A 1 cm midline incision was made at the scalp, centered approximately at lambda. An infusion burr hole was stereotactically created 1.5 mm posterior, 3.0 mm lateral to lambda using a fine drill bit for all infusions. A 22s-gauge neede attached to a 25 μL Hamilton syringe driven by a syringe pump (Bioanalytical Systems, West Lafayette, Indiana) was lowered 3.5 mm below the surface of the skull for cerebellar infusions and remained in the cerebellum parenchyma for 5 minutes before the infusion. Five minutes after the infusion, the infusion needle was slowly raised 1 mm every minute until out of the cerebellum. The burr holes

were sealed with sterile bone wax. The incision was then closed with Surgi-lock 2oc (Meridian Animal Health, Omaha, Nebraska), averaging 2 drops along the length of the incision and held together for 20 seconds. The mouse was placed under a heat source and monitored until alert and mobile. Mice had access to water containing acetaminophen (1.6mg/mL) (McNeill-PPC, Inc, Fort Washington, PA) for three days following initial dose of buprenorphine (0.05-.1mg/kg, S.C.) immediately following tumor cell infusions for pain alleviation during anesthetic recovery. The recovery method is important due to the severely impaired immune systems of these mice.

Six μL of 60,000-cells/ μL in plain DMEM (Invitrogen, Carlsbad, CA) was infused into the right cerebellum at a flow rate of 0.25 μL/min for 24 minutes. Cell implants were permitted to grow for 1 week before MRI scanning to confirm tumor formation. Tumor growth was assessed again at 14 and 21 days via MRI T1-weighted imaging, DWI and water mapping techniques. Twenty-one days post-implantation was chosen as a humane endpoint to reduce prolongation of potential distress in the animals, since it is a time-point prior to when subject mortality would be expected (28-30 days). Animals were monitored daily for signs of pain and distress and if discovered, the animals were euthanized. Cerebella were collected and sent to the Department of Anatomic Pathology at Virginia Commonwealth University, Richmond, Virginia. Cerebellum gross sections containing intact tumor were then sectioned and subjected to

neuropathological analysis to determine volume of tumor and extent of tumor cell infiltration of normal cerebellar tissue.

Subcutaneous Flank Tumor Inoculation

Animals receiving flank inoculations were not anesthetized. Cell suspensions were prepared in culture medium free of additives. Target area for inoculation was the back, midline, with needle angled in the posterior direction of the mouse. The target area was prepared with an isopropyl swab. A maximum of 200 μL total suspension (1,000,000 to 4,000,000 cells) were injected via a 28ga needle after tenting the cutaneous layer. The needle was allowed to remain in place for several seconds after injection to reduce inoculate backflow. A sterile cotton swab was applied in the target area to reduce potential bleeding. Flank inoculation with medulloblastoma cells is expected to produce palpable tumors within 6-8 days. Tumor volume was assessed at least twice a week afterward. Tumor volume was not allowed to exceed 2.5cm^3 or 10% of subject body mass. Mice bearing flank tumors were observed daily for ulceration and necrosis. If noted, the mice were euthanized.

Magnetic Resonance Imaging

Each mouse to be scanned was anesthetized by intraperitoneal administration of 100mg/kg Ketamine + 10mg/kg Xylazine (1 : 4). Lubricating veterinary ointment was applied to the eyes and the animal was placed under a heating source. Gd-DTPa was injected I.V. via tail vein for MRI to monitor

tumor growth. Each mouse was placed in an acrylic imaging tube, secured via plastic ear bars, and fitted with a surface coil. Images were acquired with a 2.4 T, 40-cm bore magnet (Bruker Medical, Inc., Billerica, MA) equipped with a 12 cm inner-diameter, actively shielded gradient insert (maximum gradient strength: 25 G/cm). An actively decoupled RF coil set was used for RF excitation/reception and was comprised of a 7 cm inner-diameter "birdcage" design resonator and a 2 cm diameter circular surface coil.

T1 images

A two-dimensional T1 imaging series was generated with a spin echo, echo-planar imaging sequence preceded by an inversion recovery preparation period using a hyperbolic secant inversion pulse. Data was obtained on 3 coronal sections are 20 mm square and at a thickness of 2.5 mm. Inversion recovery times were: 30, 60, 150, 300, 700, 1300, and 2500 msec.

Derivation of Human Derived Tumor Cells

Human Medulloblastoma xenograft derived from a tumor of a 4-year old male patient. Established under approved research protocols, and characterized in our laboratory (Pediatric Neuro-Oncology Laboratory, Virginia Commonwealth University). Samples of tumor were first obtained to allow full neuropathologic evaluation and diagnosis, as required for clinical management of the patient's disease. The site of origin of all tumor samples was cerebellum. Cells were grown in DMEM supplemented with 10% heat-inactivated fetal bovine serum,

glutamine, and 1% penicillin-streptomycin solution at 37*C temperature with 5% CO2 in a humidified incubator. All tissue culture reagents and supplements were obtained from Gibco BRL (Grand Island, NY) unless otherwise noted. Monolayers of tumor cells were typsinized, counted on a hemacytometer and viability was assessed by trypan blue exclusion. Cells were washed twice in phosphate buffered saline (PBS) and concentration was adjusted appropriately (Graf et al. 2005).

Determination of Tumor Volume from MRI

The three-dimensional volume of a tumor determined from a two-dimensional MRI scan uses the equation for the volume of a spheroid. In this equation, the volume is equal to four times the radius cubed, all divided by three. Replacing the radius with the diameter divided by two, and making the diameter cubed equal to the width of the tumor times the height of the tumor times the width of the MRI slice, gives a simplified equation for volume. The volume of a spheroid can be estimated as the width of the tumor times the height of the tumor times the slice width, all divided by two (π/6 being approximately ½).

$$\text{Volume} = (4\pi r^3)/3 \qquad r = d/2$$

$$= (4\pi d^3)/(8*3)$$

$$d^3 = \text{Width} \times \text{Height} \times \text{Slice Width}$$

$$\text{Volume} = (W \times H \times SW)/2$$

Quantification of VC312 mRNA levels

Total RNA was isolated from VC312 tumor tissue using TRIzol reagent, using the manufacturer's protocol (Invitrogen, CA) and standard extraction protocol (Sambrook and Russell, 2001). To prepare tissue extracts for RNA isolation, flash frozen pieces were ground to a fine powder with a frozen mortar and pestle prior to being added to TRIzol reagent. RNA was quantified using spectrophotometry to assess concentration of the RNA in the extracts and treated with RQ1 DNase (Promega, Madison, WI) using the manufacturer's protocol.

Western blot analysis for phosphorylated and total AKT

Cultured adherent cells in T-75 flasks were washed with PBS and incubated with 1 ml of ice-cold RIPA lysis buffer (50 mM Tris-HCl, 150 NaCl, 0.5% SDS, 1% sodium deoxycholate, 1% Nonidet p-40) for 5 minutes on ice with gentle agitation. Cells were scraped from flasks, sheared with 26.5 gauge needle and centrifuged at 16000 rpm for 30 minutes at 4°C. Supernatant was collected and stored at -80°C until use. Alternatively, frozen tumor tissue samples from primary medulloblastoma samples were thawed and suspended in 800 µL ice-cold RIPA buffer containing protease inhibitor cocktail (Calbiochem, San Diego, CA) and mechanically homogenized. The homogenized tissue was incubated at 4°C for 15 minutes and centrifuged at 16000 rpm for 30 minutes at

4°C. Protein supernatants were aliquoted and stored at -80°C until use. Proteins were quantified using the Lowry method and BioRad DC reagent (BioRad, Hercules, CA) using the manufacturer's protocol. A BSA (Pierce, Rockland, IL) standard curve was used (25µg/ml to 2000µg/ml range). Equal amounts of protein were loaded onto Bis-Tris 4-12% density gradient gels (Invitrogen, Carlsbad, CA) for SDS-PAGE at 120 V using the manufacturer's power source and protocol (Novex). Proteins were transferred (1 hour at 30V) onto nitrocellulose (Invitrogen) and incubated with 15 ml blocking buffer [5% bovine milk in Tris-buffered saline (50 mM Tris, pH 7.6, 150 NaCl) plus 0.05% Tween-20] for 1 hour at room temperature with gentle agitation. Primary antibody [anti-Phospho-AKT (1:2000), Pan-AKT (1:2000) and anti-beta-actin (1:2000)] were added to 10 ml blocking buffer and incubated overnight at 4°C with gentle agitation. Membranes were washed with rinse buffer [Tris buffered saline (50 mM Tris, pH 7.6, 150 NaCl) plus 0.05% Tween-20] for 6 x 5 minutes with vigorous agitation. HRR-conjugated secondary antibody was added to 10 ml blocking buffer (1:3000,) and incubated for 1 hour at room temperature with gentle agitation. Membranes were washed as before and developed using enhanced chemiluminescence (ECL) reagents (Amersham Biosciences, Piscataway, NJ) and the manufacturer's protocol. Immunoreactivity was visualized by exposure to autoradiography film (Marsh) and was developed using an X-OMAT developer (Kodak, Rochester, NY). For quantitative analysis, optical

densities of autoradiographic bands were measured using ImageQuant™ software (Amersham Biosciences, Piscataway, NJ).

Determination of Tumor Volume from Caliper measurements

The volume of subcutaneous tumor volumes is an important tool in assessing disease growth and effectiveness of therapeutics. Manual calipers are used as a noninvasive technique for measuring tumor volume. The 2 longest perpendicular axes of each xenograft tumor were measured to the nearest 0.1 mm by an investigator familiar with collecting caliper measurements of xenograft tumors in mice. The depth was assumed to be equivalent to the shortest of the perpendicular axes, defined as *y* (Tomayko et al, 1989; Euhus et al, 1986).

$$\text{Xenograft Tumor Volume} = xy^2 / 2.$$

In Vivo Analysis of Effects of Perifosine on VC312 Tumor Growth

Groups of mice were inoculated with VC312 tumor cells as described previously. When the mice reached post-inoculation day 15 with measurable tumors, perifosine-containing (36 mg/kg/d) or placebo drinking water was refreshed every 48 hours for up to 20 days by (n = 4 mice per group). An amount of 15 mg of Perifosine was weighed and dissolved in 100 mL of sterile water. Average daily water consumption was 5 ml per day, resulting in an average daily dose of 36 mg/kg/d or 252 mg/kg/wk. The dimensions of the resulting tumors were determined at least three times per week using a digital caliper, and the tumor volume (cubic millimeter) was calculated as described

above. The mice were sacrificed by asphyxiation with regulated CO_2, and the tumors were excised, snap frozen in liquid nitrogen then transferred to a freezer at –80°C, until use. Protein extracts from the tumors were used to assess the phosphorylation status of AKT. To determine the effect of perifosine on survival, we counted the days from the date the treatment (perifosine or control) was begun to the time the control cohort of mice were sacrificed or to the end of the perifosine treatment or until euthanasia, as described previously (Zhijie et al, 2010).

Chapter 4

Results

Creation of Intracerebellar Medulloblastoma Murine Model

The Medulloblastoma cell line VC312 was derived from a tumor of a 4-year-old male patient. The primary culture (VC312) of MB was derived from a tumor of a 2-year old male patient treated at the Virginia Commonwealth University Health System's Medical College of Virginia Hospital under an IRB approved protocol. Briefly, samples of the tumor were first obtained to allow full neuropathologic evaluation and diagnosis, as required for the clinical management of the patient's disease. The sterile dissection of tumor biopsy was dissociated and plated in 6-well tissue culture plates and expanded in DMEM/F12 medium supplemented with 1% N-2 supplement (Invitrogen), 5% FBS, 20 ng/ml recombinant human EGF and 10 ng/ml recombinant human bFGF (Beckton Dickenson). VC312 cells were subsequently maintained in DMEM (with L-glutamine) supplemented with 10% FBS.

Volume of Tumor Injection

The proper volume of inoculum had to be determined in order to induce reliable tumor formation within a relatively brief time course, but without undesirable adverse effects on the recipient animals. It was decided that roughly 10% of the total cerebellar volume would be an acceptable maximum initial tumor cell infusion, so as to avoid adverse effects of the relatively rapid infusion process. Thus, based upon the average athymic nude female mouse cerebellum volume being approximately 60 μL (Airey et al. 2001), we concluded that 6 μL would be the volume of the tumor inoculum. The tumor cell concentration for the inoculum was determined from previous experiments performed in our lab as being a maximum concentration without blocking the fine needle of the Hamilton syringe (Nottingham 2008). This concentration is equal to 50,000 cells per μL, which amounts to 300,000 VC312 cells per injection.

Establishment of tumor inoculum into cerebellum

Our lab has completed orthotopic cancer experiments in the past but never in the cerebellum. Therefore, proper stereotactic coordinates using the athymic mouse skull sutures had to be established. Using the Mouse Brain Atlas (mbl.org)(Figure 4-1) it was determined that 1.5 mm posterior from Lambda, 3.0mm lateral and 3.0 mm deep would place the inoculum in the right hemisphere of the posterior lobe of the cerebellum.

The growth of VC312 xenograft tumor in the cerebellum was confirmed with MRI (Figure 4-2) and dissection of the mouse brain. Once the growth of

the human tumor-derived cell line was confirmed, the development of an *in vivo* growth pattern for a primary medulloblastoma in the mouse cerebellum could begin.

Hematoxylin and Eosin Staining

Hematoxylin and Eosin (H&E) stains were performed on representative formalin-fixed, paraffin embedded tissue sections from representative animals from all stereotactic infusion parameters by the VCU Anatomic Pathology Research Services.

Tumor Bearing Mice

Consistent results were observed among all tumor-bearing mice, and as with the stereotactic infusions, the region of interest was the right cerebellum.

On MRI (Figure 4-2), Gd-enhanced T1-weighted imaging qualitatively showed tumor enhancement in the cerebellum and around the brain stem.

Figure 4-1. Scaled Image from Mouse Brain Atlas. Image illustrates the location of Lambda (lj) as the intersection of the sagittal and lambdoid sutures. The burr hole was positioned: 1.5 mm anterior, 2.5 mm lateral to lambda, and the inoculum was positioned 3.0 mm ventral to the burr hole placement. placing the VC312 cells in the lateral portion of the cerebellum.

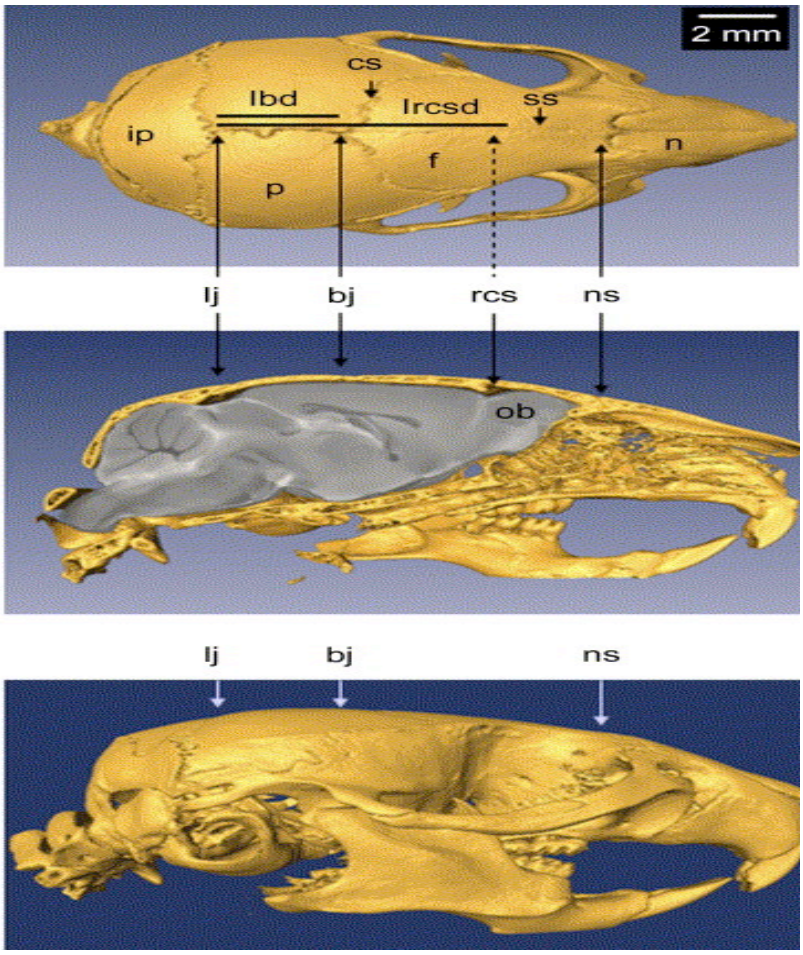
2 mm
cs
lbd
lrcsd
ss
ip
f
n
p
lj
bj
rcs
ns
ob
lj
bj
ns

Figure 4-2. Gd-enhanced T1-weighted MRI of an animal on Day 17 Post Implantation. The image demonstrates a coronal slice from the mouse cerebellum. The tumor boundary is visible as hyper-intensity seen in the lateral aspect of the cerebellum.

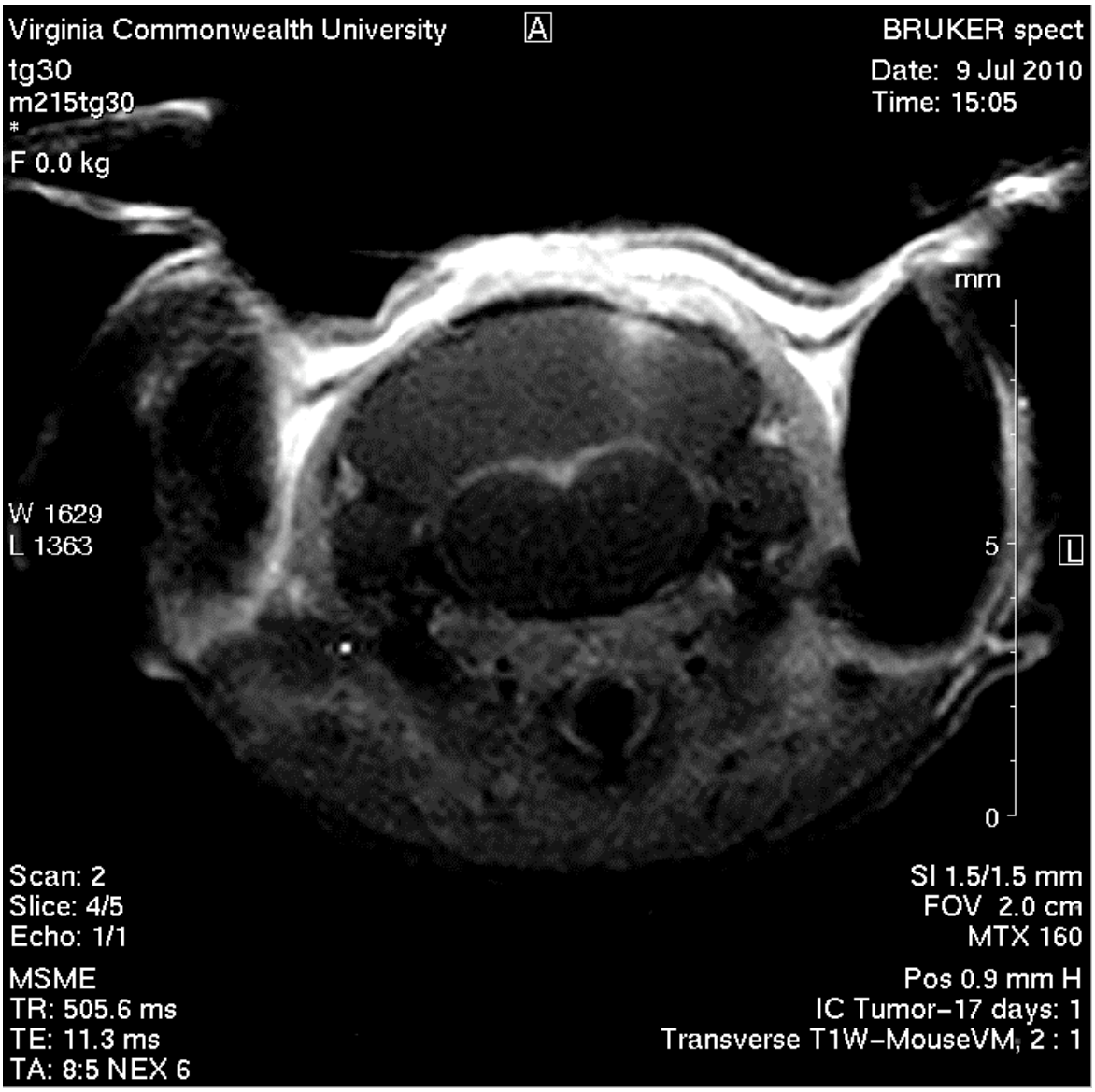
Virginia Commonwealth University
A
BRUKER spect
tg30
Date: 9 Jul 2010
m215tg30
Time: 15:05
*
F 0.0 kg
mm
W 1629
L 1363
5
L
0
Scan: 2
Slice: 4/5
Echo: 1/1
SI 1.5/1.5 mm
FOV 2.0 cm
MTX 160
MSME
TR: 505.6 ms
TE: 11.3 ms
TA: 8:5 NEX 6
Pos 0.9 mm H
IC Tumor–17 days: 1
Transverse T1W–MouseVM, 2 : 1

The tumor growth in the intracerebellar model was measured using a formula for the volume of a spheroid (described in the Methods section) at 7 days, 14 days, 21 days and 28 days post-implantation. The average growth of the MB in the nude mouse cerebellum can be seen in Figure 4-3.

Consistent results were observed in the flank tumor bearing mice, the region of interest was the flank region and the subcutaneous growth of the tumor (Figure 4-4). The dimensions of the tumors were measured using a caliper every third day.

Histology of Tumor

The representative histological images of the *in vivo* tumors can be seen in figure 4-5. The tumor is very cellular, with many mitoses and little cytoplasm. The cells appear to form clusters and rosettes.

Figure 4-3. Volumetric Growth of Murine Intracerebellar MB.

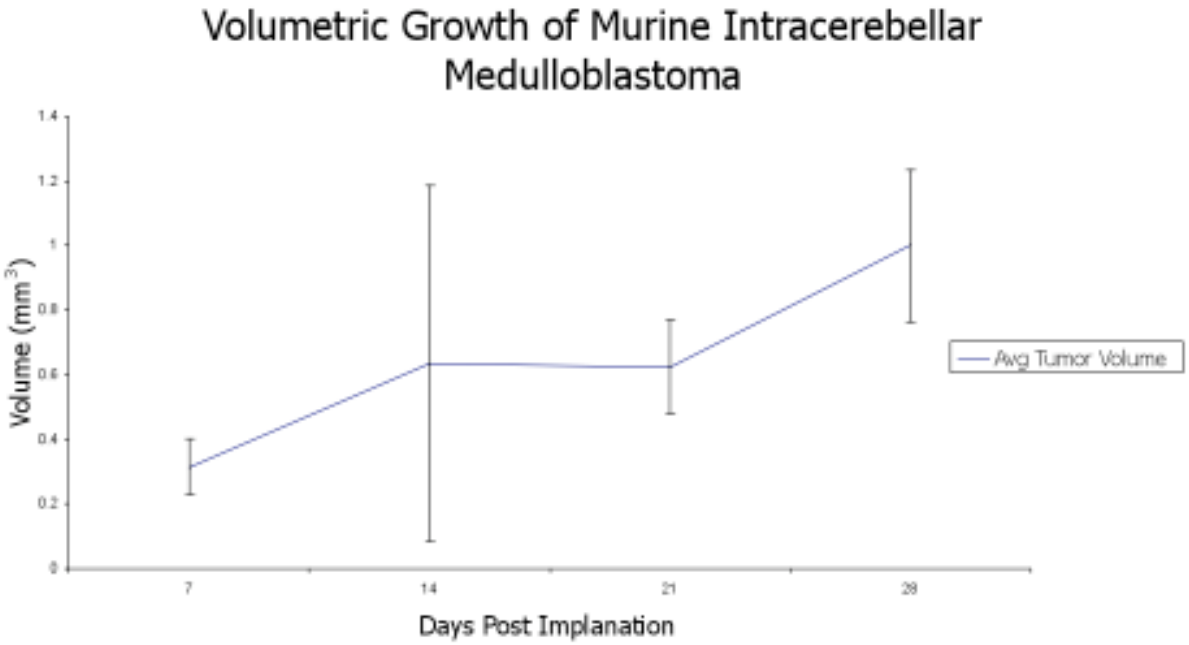
Volumetric Growth of Murine Intracerebellar Medulloblastoma
Volume (mm3)
1.4
1.2
1
0.8
0.6
0.4
0.2
0
7
14
21
28
Days Post Implanation
Avg Tumor Volume

Figure 4-4. Image of a subcutaneous VC312 flank tumor.

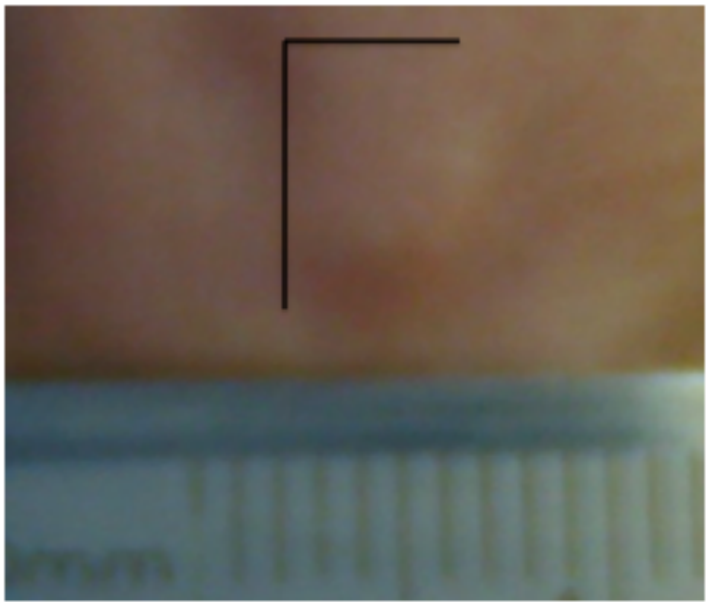

Figure 4-5. Histology of Intracerebellar and Flank VC312 Tumors.

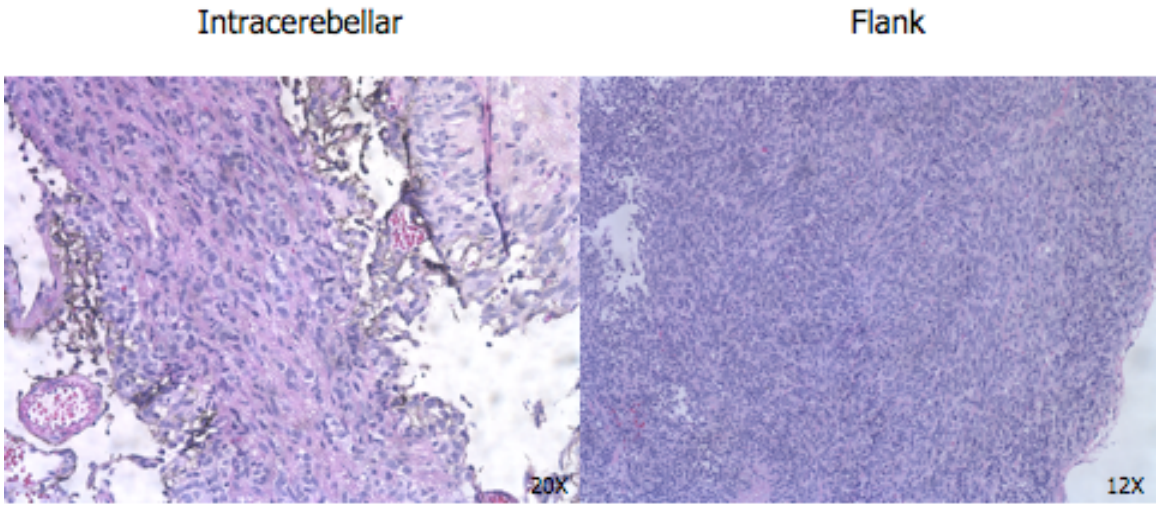
Intracerebellar
Flank
20X
12X

The Effect of Perifosine on Medulloblastoma cells in vitro

Previous work by Dr. Anil Kumar in this laboratory studied the effect of the therapeutic agent Perifosone on different MB cell lines *in vitro* (Kumar et al., 2009). His data showed that endogenous active AKT is present at high levels compared with normal brain samples in MB and derivative cell lines. Treatment of the MB with perifosine decreases the active AKT levels in a dose-dependent and time-dependent manner. He also showed that perifosine treatment led to rapid decreases in cell survival in tumor cells. Dr. Kumar also reported that exposure to etoposide and radiation followed with perifosine resulted in greater thant additive effect on cell death. These results indicate that perifosine, either alone or in combination with other drugs, might be an effective therapeutic agent for the treatment of MB. These results highlight the potential value of studying of the effects of Perifosine in an *in vivo* model.

The Effect of Perifosine on Medulloblastoma in vivo

Treatment of tumor bearing mice resulted in a decrease of overall tumor volume in both intracerebellar and flank models. The intracerebellar-implanted mice were given perifosine treatment beginning sixteen days post-implantation. The volumetric growth of the intracerebellar implanted MB appears sporadic initially (Figure 4-6A). However, the effect of perifosine begins to appear when the tumor volumes are separated into treated and untreated groups and their

volumes are averaged (Figure 4-6B). Finally, when the tumor volumes are normalized to the size of the tumor upon initial inspection with MRI (day 7), the effect of perifosine within the treatment group was significant (figure 4-7).

The effect of perifosine on the growth of the flank tumor model is illustrated in Figure 4-8. The tumor sizes were normalized to the size of the tumor at the beginning of treatment and averaged. The effect of perifosine is significant from eight days post-treatment until the end of the study.

The intracerebellar-implanted mice were given perifosine treatment following the MRI at day 14. At day 35 post implantation only the four mice treated with perifosine remained alive. Using a Fisher's exact test to evaluate the significance, the effect of perifosine on the survival of intracerebellar-implanted mice is significant (Table 4-1).

The effect of perifosine on the signaling pathways of MB is illustrated in figure 4-9 by the suppression of active AKT in treated versus untreated MB flank tumors. Qualitative effects of perifosine on the histology of the tumor are illustrated in the decreased density of stained cells. Further, when the tumors were stained with Ki-67, a cellular marker for proliferation, the Ki-67 sections showed qualitative differences between the treated and untreated tumors. The treated tumor sections displayed a lower density of Ki—67 positive cells than the untreated tumor sections. Therefore, perifosine effectively suppressed the proliferation of MB cells in the treated animal model.

Figure 4-6. Effect of Perifosine on Growth of Murine Intracerebellar Medulloblastoma. A. The volumetric growth data for each intracerebellar-implanted mouse are plotted individually. B. The average volumetric growth rates for perifosine-treated vs untreated mice are demonstrated.

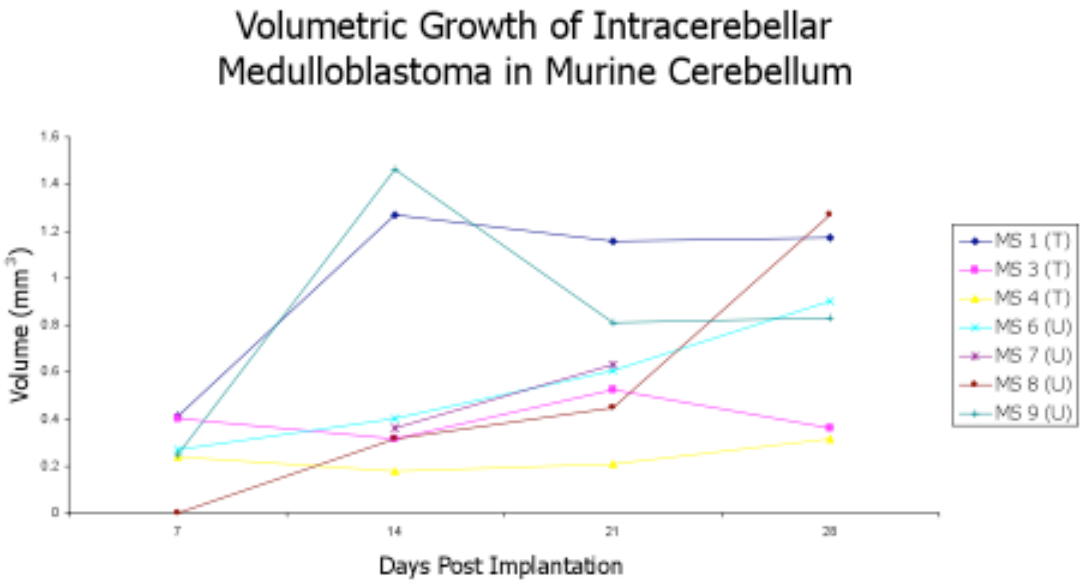
Volumetric Growth of Intracerebellar Medulloblastoma in Murine Cerebellum
Volume (mm 3)
Days Post Implantation
MS 1 (T)
MS 3 (T)
MS 4 (T)
MS 6 (U)
MS 7 (U)
MS 8 (U)
MS 9 (U)

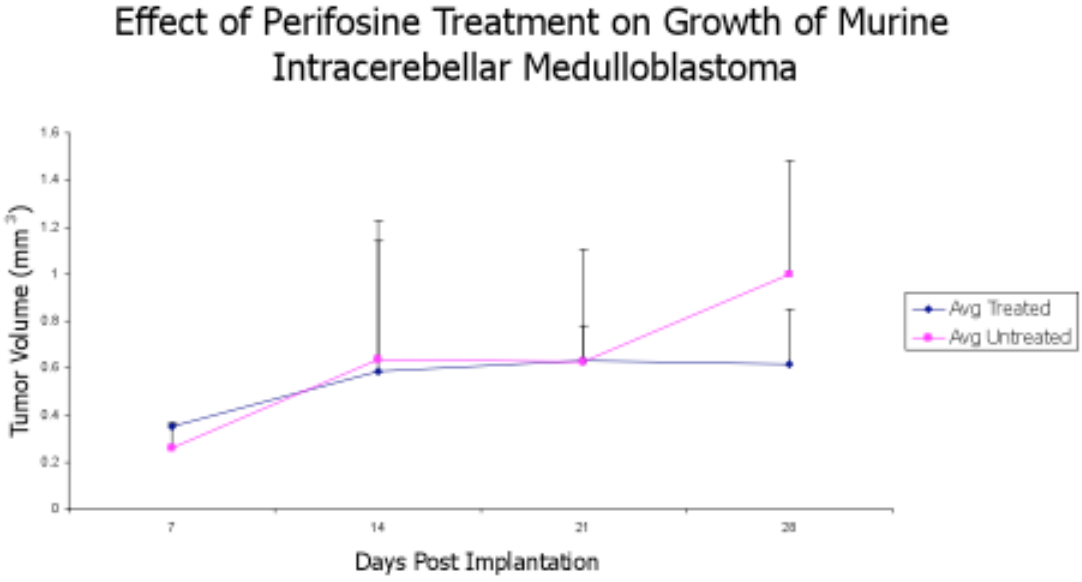
Effect of Perifosine Treatment on Growth of Murine Intracerebellar Medulloblastoma
Tumor Volume (mm 3)
Days Post Implantation
Avg Treated
Avg Untreated

Figure 4-7. The Effect of Perifosine on the growth of murine intracerebellar medulloblastoma. Treatment with perifosine began on day 17 post-implantation. Tumor volumes have been normalized to the volume of the tumor at initial MRI inspection on day 7 post implantation.

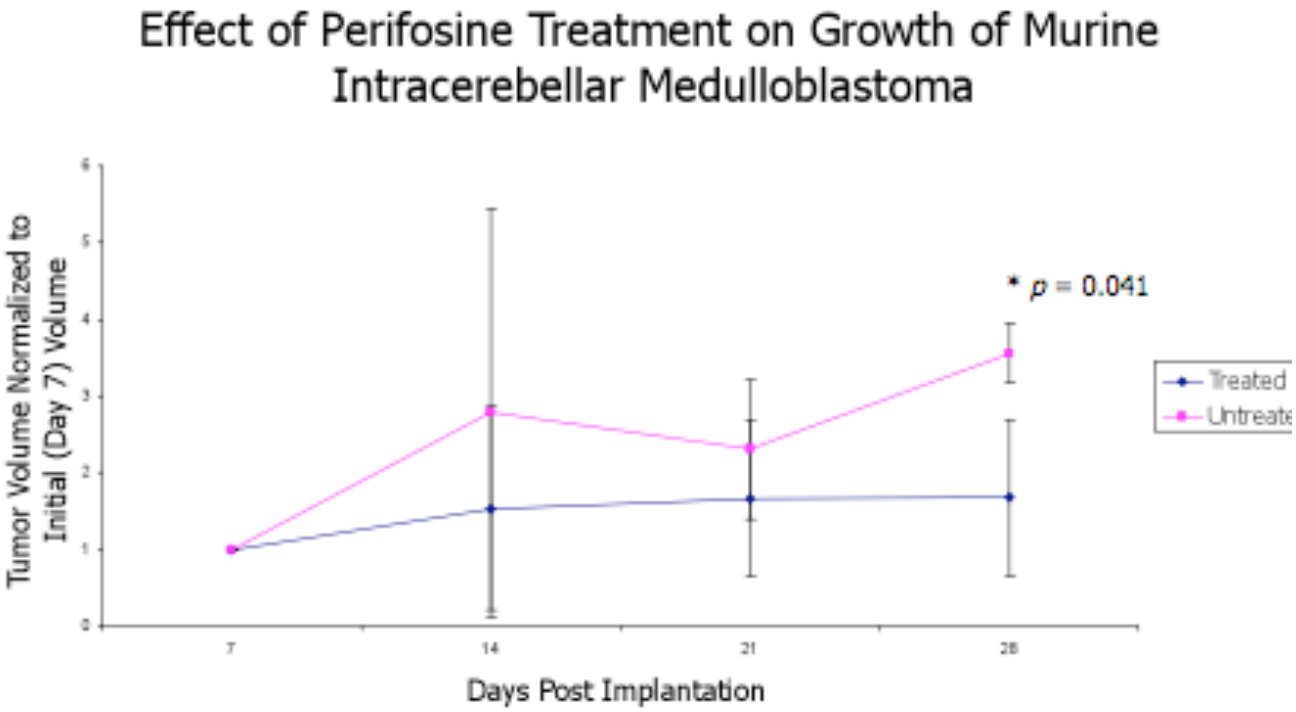
Effect of Perifosine Treatment on Growth of Murine Intracerebellar Medulloblastoma
Tumor Volume Normalized to Initial (Day 7) Volume
* p = 0.041
Treated
Untreate
7
14
21
28
Days Post Implantation

Figure 4-8. Effect of Perifosine Treatment on Growth of Medulloblastoma Flank Tumors. Tumor volumes have been normalized to the volume of the tumor at the beginning of treatment.

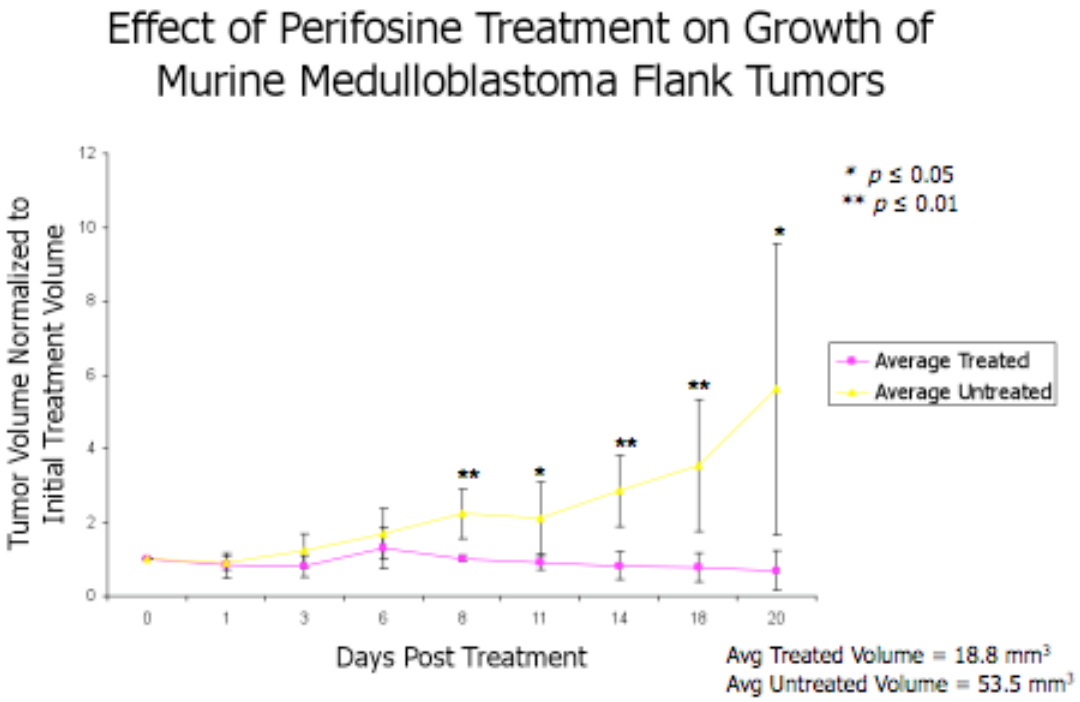
Effect of Perifosine Treatment on Growth of Murine Medulloblastoma Flank Tumors
Tumor Volume Normalized to Initial Treatment Volume
Days Post Treatment
* p ≤ 0.05
** p ≤ 0.01
Average Treated
Average Untreated
Avg Treated Volume = 18.8 mm3
Avg Untreated Volume = 53.5 mm3

Table 4-1. Effect of Perifosine on Survival of Mice with intracerebellar implantation of Medulloblastoma.

Effect of Perifosine on Survival of Mice with Intracerebellar Medulloblastoma Day 35 Post Implantation *

	Untreated	Treated with Perifosine
Alive	0	4
Moribund/Dead	4	0

* $p = 0.028$

Treatment initiated post implantation day 16

Figure 4-9. Suppression of active AKT by perifosine in VC312 flank tumors. Flank tumor-bearing mice were treated with perifosine for 20 days and the cell lysates were then subjected to Western blot analysis.

Effect of Perifosine on p-AKT

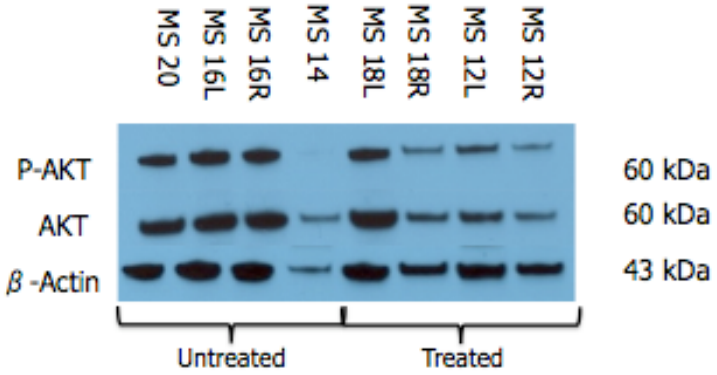

Effect of Perifosine on p-AKT vs total AKT in treated and untreated tumors

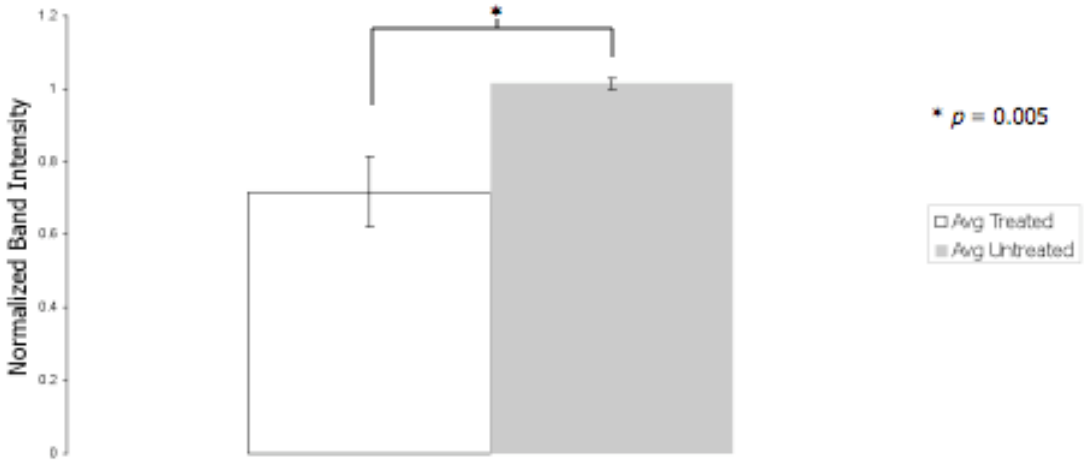

Figure 4-10. The effect of perifosine on the histology of medulloblastoma in a flank tumor model. A. Hematoxylin and eosin staining of treated and untreated tumor sections. B. Flank tumor sections stained for Ki-67, a marker for cellular proliferation.

A

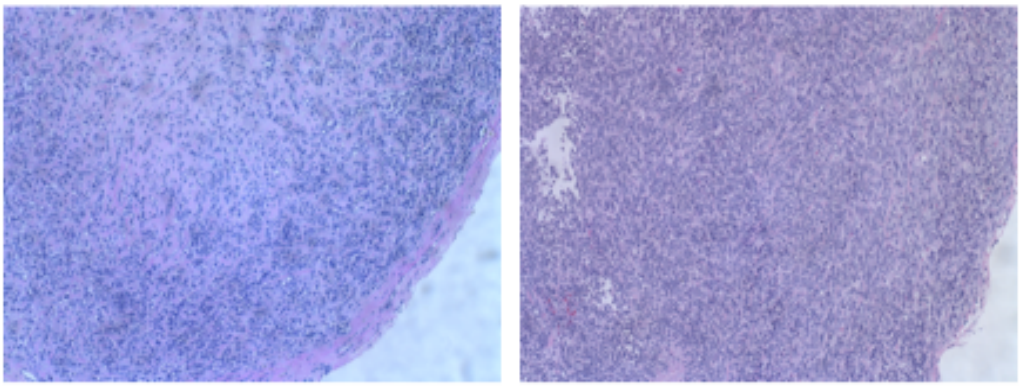
Effect of Perifosine on Histology
Treated
Untreated

B

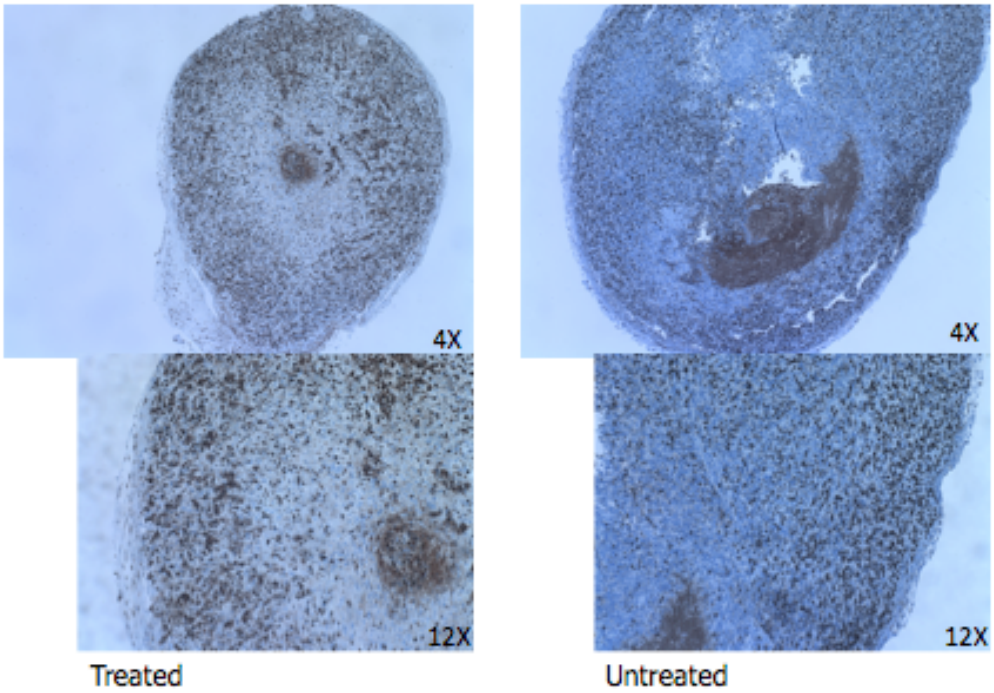
Effect of Perifosine on Ki-67 levels on treated and untreated medulloblastoma flank tumors
4X
12X
4X
12X
Treated
Untreated

Chapter 5

Discussion

The medulloblastoma is the most common malignant pediatric brain tumor, and is still associated with mortality and severe side effects from clinical treatment (Packer et al., 2003). The development of a clinically relevant *in vivo* model is important not only to further understand the disease but also to provide a new and improved means with which to test novel therapeutics. The standard *in vitro* experimental models of human cancer cell lines do not accurately replicate the conditions, three-dimensional interaction or microenvironment that a tumor experiences *in vivo* and orthotopically.

Current models of replicating MB include genetically engineered animal models (Hatton et al., 2008) and orthotopic xenograft models (Kessler et al., 2009). These models fail to use a human tumor cell line, which reduces their usefulness for studying therapies designed for humans. Further, the clinical effectiveness of novel therapeutic strategies can more accurately be predicted when human tumor-derived cell lines are used in an orthotopic xenograft model (Hoffman et al., 1999).

Previous intracerebellar xenograft models have been established in SCID mice, systematically developed and broadly characterized for multiple established MB cell lines (Qin et al., 2006) excluding VC312. However, these models have the serious limitation of using established cell lines that have a homogeneous cell population, uniform growth rate and hypersensitivity to therapy (Qin et al., 2008). The development and volumetric characterization using MRI of an orthotopically implanted primary human MB tumor has not been reported.

In this study, we described the establishment of an intracerebellar model in athymic nude mice with cells cultured from a primary human tumor. Utilizing MRI and a flank tumor model to establish the volumetric growth of the tumor *in vivo* we evaluated the preclinical effectiveness of the anti-AKT activities of perifosine, an established anti-cancer drug that has been taken to phase II clinical trials for peripheral cancers (Gills and Dennis, 2009). Our lab had previously studied the *in vitro* effects of perifosine and showed that it possessed potent suppression of AKT signaling activity by decreasing cancer cell survival and growth (Kumar, et al., 2009). The literature documents that the phosphatidylinositol 3′-kinase (PI3K)–mediated AKT signaling pathway has been found to have a role in tumor proliferation and survival (Vivanco et al., 2002), making the AKT signaling pathway a valuable target for anti-tumor therapeutics. Further, elevated activation of PI3K/AKT signaling pathways has been found in MB (Hartmann et al., 2006).

Repeated MRI scans illustrated volumetric growth and histopathological features similar to the primary tumor which confirmed successful establishment of an intracerebellar MB model in nude mice. Using this model, we showed the effect of perifosine on suppressing tumor growth both in the orthotopic intracerebellar model and in the flank model. Perifosine also effectively increased survival of mice bearing intracerebellar tumors. Further, perifosine effectively suppressed active AKT signaling and reduced the density of proliferating cells in vivo.

An advantage of xenograft models is that the relative tumor growth dynamics can roughly be predicted by the concentration of tumor cells implanted (Lampson et al., 2001). Therefore, identical cell concentrations implanted in the same stereotactic position in the cerebellum would theoretically grow at the same rate. A further advantage of such a xenograft model would be to allow objective measurement of the effectiveness of chemotherapy or other therapeutic strategies. Unfortunately, we found there to be a large variation in the volumetric growth rates at days 14 and 21 post implantation. However, by the end of the study, the sizes of the tumors measured from the MRI scans were approximately similar, while the overall rates of growth of individual tumors showed variability.

While faithful reproduction of intracerebellar MB tumors was not confirmed with histology, leptomeningeal dissemination was evident in both the MRI scans and the prepared histology. It should be noted that this corresponds

to a troubling clinical characteristic of MB in humans, with dissemination early in its course. The murine model of intracerebellar MB established in this study thus appears to replicate dissemination in the CNS, especially around the brainstem. This may be a valuable model for novel therapeutic strategies targeting leptomeningeal dissemination of MB. It is notable in this regard that despite prominent leptomeningeal dissemination in these animals, the group receiving perifosine had a significantly longer survival. This provides significant hope that this therapeutic strategy could be effective against MB even in patients who have developed leptomeningeal spread of their tumor.

Limitations of our model included the culturing of the primary tumor prior to implantation. While the cell cultures of the MB used in the study were limited to less than five passages, the *in vitro* culturing could have had an effect on the heterogeneity of the cell population. The homogeneous cell population would make for uniform growth and the possibility of sensitivity to therapy (Kamb et al., 2005). A solution to this problem would be the implantation of freshly resected tumor pieces intracerebellarly, however due to the availability of the resected samples, cultured primary tumor cells were the best option. Another issue that should be addressed is the location of the tumor implantation. The majority of MBs grow from the vermis of the cerebellum, the site of massive cellular differentiation during development. The implantation was positioned in the right hemisphere of the lateral lobe of the cerebellum because it was the only feasible target in the cerebellum. Due to the size of the cerebellum in these

animals, it was far too difficult to position the implantation in the vermis. Further, the mice used in the study were young adults (4-6 weeks) whose cerebellar development was mostly complete, potentially reducing the microenvironment difference between vermis and lateral hemisphere.

Future studies with this model approach would be appropriate to address a number of issues highlighted by this work, to improve and extend the important findings here. In particular the stereotactic refinement, tumor reproducibility and perifosine dose optimization. Refining the stereotactic coordinates would improve the reproducibility of the model in the cerebellum. Proper tumor implantation is the keystone of this model, continuing to optimize the surgical protocol will allow extension of this model to explore signaling, angiogenesis and dissemination of the disease. Further, faithful orthotopic implantation and growth of the primary human MB in the cerebellum allows the further characterizing of the complexities of this tumor; it will also permit refinement of the perifosine growth suppression mechanism *in vivo*.

In order to improve reproducibility; the size and age of mice used in the model need to be standardized. The volume of the cerebellum varies with each subject and therefore proper implantation location can fluctuate. Correlating the stereotactic coordinates to the size and age of the animal should improve the accuracy of the implantation and the model's orthotopic fidelity.

Maximum anti-tumor effect while maintaining increased survival benefits is the goal of perifosine dose optimization. Exploring the time dependence of perifosine effectiveness is a logical extension of the therapeutic enhancement. Further, characterizing the suppression of subarachnoid growth will improve the understanding of the survival benefits of perifosine.

Finally, optimization of the intracerebellar MB model will allow utilization of the approaches learned in this work to be applied to newly obtained primary tumor samples of MB.

Literature Cited

Airey et al. (2001) Genetic Control of the Mouse Cerebellum, The journal of Neuroscience; 21(14): 5099-5109.

American Cancer Society (ACS). Atlanta (GA): U.S. Department of Health and Human Services, Centers for Disease Control and Prevention, National Center for Chronic Disease Prevention and Health Promotion; 2009. Available at: http://www.cdc.gov/cancer/npcr/.

Brown HG et al. (2000) "Large cell/anaplastic" medulloblastomas: a Pediatric Oncology Group Study. J Neuropathol Exp Neurol 59: 857–865.

Buckner JC, Brown PD, O'Neill BP, Meyer FB, Wetmore CJ, Uhm JH. (2007) Central nervous system tumors. Mayo Clin Proc; 82(10):1271-1286.

Canettieri G, Di Marcotullio L, Greco A et al. (2010) Histone deacetylase and Cullin3-REN(KCTD11) ubiquitin ligase interplay regulates Hedgehog signalling through Gli acetylation. Nat Cell Biol; 12(2):132-42.

Eberhart CG. (2007) In search of the medulloblast: neural stem cells and embryonal brain tumors. Neurosurg Clin N Am; 18(1):59-69.

Euhus DM, Hudd C, LaRegina MC, Johnson FE. (1986) Tumor measurement in the nude mouse. J Surg Oncol; 31: 229–234.

Fan, Xing and Charles G. Eberhart. (2008) Medulloblastoma Stem Cells. Journal of Clinical Oncology; 26:2821-2827.

Fouladi M et al. (1999) Comparison of CSF cytology and spinal magnetic resonance imaging in the detection of leptomeningeal disease in pediatric medulloblastoma or primitive neuroectodermal tumor. J Clin Oncol 17: 3234–3237.

Fults DW. (2005) Modeling Medulloblastoma With Genetically Engineered Mice. Neurosurg Focus;19(5).

Giangaspero F et al. (1999) Medulloblastoma with extensive nodularity: a variant with favorable prognosis. J Neurosurg 91: 971–977.

Gilbertson RJ, Ellison DW. (2008) The Origins of Medulloblastoma Subtypes. Annual Review of Pathology: Mechanisms of Disease; 3:341-365.

Gilhuis J, van der Laak JAWM, Pomp J, Kappelle AC, Gijtenbeek JMM, Wesseling P. (2006) Three-dimensional (3D) reconstruction and quantitative analysis of the microvasculature in medulloblastoma and ependymoma subtypes. Angiogenesis; 9:201–208.

Gills JJ and Dennis PA. (2009) Perifosine: An update on a novel Akt Inhibitor. Curr Oncol Rep; 11(2): 102-10.

Gurney JG and Kadan-Lottick N (2001) Brain and other central nervous system tumors: rates, trends, and epidemiology. Curr Opin Oncol 13: 160–166.

Halperin EC et al. Pediatric Radiation Oncology. Philadelphia: Lippincott Williams and Wilkins, 2005.

Hartmann W, Digon-Söntgerath B, Koch A, et al. (2006) Phosphatidylinositol 3′ kinase/AKT signaling is activated in medulloblastoma cell proliferation and is associated with reduced expression of PTEN. Clin Cancer Res; 12: 3019–27.

Hatton, Villavicencio, Tsuchiya et al. High Medulloblastoma Incidence in Smo/Smo Mouse Model. Cancer Res 2008;68(6):1768–76.

Kamb A. (2005) What's wrong with our cancer models? Nat Rev Drug Discov; 4:161–5.

Katoh Y, Katoh M. (2009) Hedgehog target genes: mechanisms of carcinogenesis induced by aberrant hedgehog signaling activation. Curr Mol Med;9(7):873-86.

Kleihues P, Burger PC, Scheithauer BW. (1993) The new WHO classification of brain tumours. Brain Pathology 3:255-68.

Kumar A, VanMeter, T. (2009) The Alkylphospolipid Perifosine induces Apoptosis and p21-Mediated Cell Cycle Arrest in Medulloblastoma. Mol Cancer Res. 7:1813.

Lampson LA. (2001) New Animal Models to probe brain tumor biology, therapy and immunotherapy: Advantages and remaining concerns. J Neurooncol; 53:275-87.

Liang X, Diehn M, Bolleb AW, Isreal MA, Gupta N. (2008) Type I collagen is overexpressed in medulloblastoma as a component of tumor microenvironment. Neurooncol; 86:133-141.

MacDonald, T. (2010) Oncology: Medulloblastoma. Emedicine. Medscape.

Momota H, Nerio E, Holland EC. (2005) Perifosine inhibits multiple signaling pathways in glial progenitors and cooperates with temozolomide to arrest cell proliferation in gliomas in vivo. Cancer Res; 65(16):7429-35.

Northcott, Paul A. Medulloblastoma comprises four distinct diseases. Abstract AACR. June 2010.

Nottingham, C. (2008). Modeling Pure Vasogenic Edema in the Rat Brain. 7-25-2008. Ref Type: Thesis.

Packer RJ *et al*. (2003) Medulloblastoma: present concepts of stratification into risk groups. Pediatr Neurosurg 39: 60–67

Packer, RJ. (1999) Medulloblastoma: Clinical and biologic Aspects. Neuro-Oncology; 1: 232–250.

Polkinghorn WR, Tarbell NJ. (2007) Medulloblastoma: Tumorigenesis, Current Clinical Paradigm, and Efforts to Improve Risk Stratification. Nat Clin Pract Oncol;4(5):295-304.

Pullen, Nicholas. The influences of Matrix Metalloproteinase-1 Expression on Glioblastoma Pathology. 4-12-2010 Ref Type: Thesis/Dissertation.

Qin Shu, Barbara Antalffy, Jack Meng Feng Su, Adekunle Adesina, Ching-Nan Ou, Torsten Pietsch, Susan M. Blaney, Ching C. Lau, and Xiao-Nan Li. (2006) Valproic Acid Prolongs Survival Time of Severe Combined Immunodeficient Mice Bearing Intracerebellar Orthotopic Medulloblastoma Xenografts. Clin Cancer Res;12:4687-4694.

Qin Shu, Kwong Kwok Wong, et al. (2008) Direct Orthotopic Transplantation of Fresh Surgical Specimen Preserves CD133 Tumor Cells in Clinically Relevant Mouse Models of Medulloblastoma and Glioma. Stem Cells; 26:1414 –1424.

Ribi K, Relly C, Landolt MA, Alber FD, Boltshauser E, Grotzer MA. (2005) Outcome of medulloblastoma in children: long-term complications and quality of life. Neuropediatrics; 36:357–65.

Tiobo NA, Lu K, Ai X, Haines GM, Emerson CP. (2006) Phosphoinositide 3-kinase and Akt are essential for Sonic Hedgehog signaling. PNAS; 103(12): 4505-4510.

Rorke LB. (1983) The cerebellar medulloblastoma and its relationship to primitive neuroectodermal tumors. J. Neuropathol. Exp. Neurol. 42:1–15.

Rudin CM, Hann CL et al. (2009) Treatment of medulloblastoma with hedgehog pathway inhibitor GDC-0449. N Engl J Med. 2009 Sep 17;361(12):1173-8.

Thorarinsdottir HK, Rood B, Kamani N, Lafond D, Perez-Albuerne E, Loechelt B, Packer RJ, MacDonald TJ. (2007) Outcome for Children <4 Years of Age With Malignant Central Nervous System Tumors Treated With High-Dose Chemotherapy and Autologous Stem Cell Rescue. Pediatric Blood Cancer; 48: 278-284.

Tomayko MM, Reynolds CP. (1989) Determination of subcutaneous tumor size in athymic (nude) mice. Cancer Chemother Pharmacol; 24:148–154.

Vivanco I, Samyers CL. The phosphatidylinositol 3-kinase AKT pathway in human cancer. Nat Rev Cancer 2002; 2:489-501.

Weiner HL, Bakst R, Hurlbert MS, Ruggiero J, Ahn E, Lee WS, Stephen D, Zagzag D, Joyner AL, Turnbull DH. (2002) Induction of Medulloblastomas in Mice by Sonic Hedgehog, Independent of Gli1. Cancer Research; 62: 6385-6389.

Xiumei Zhao et al. Global gene expression profiling confirms the molecular fidelity of primary tumor-based orthotopic xenograft mouse models of medulloblastoma. 4-20-2010. Ref type: Abstract.

Zhijie Li, Fei Tan, David J. Liewehr, Seth M. Steinberg, and Carol J. Thiele. (2010) In Vitro and In Vivo Inhibition of Neuroblastoma Tumor Cell Growth by AKT Inhibitor Perifosine. J Natl Cancer Inst 102: 758-770.

Vita

Thomas Sanderson Gavigan was born on February 4, 1979, in Washington, District of Columbia, and is an American citizen. He graduated from Charlotte Country Day School, Charlotte, North Carolina, in 1998. In 2002, he received his Bachelor of Science in Biology from the University of North Carolina, Chapel Hill, North Carolina. He participated in research at the University of North Carolina Hospitals, Chapel Hill, North Carolina, in the labs of Dr. David Gerber and Dr. Kim Isaacs.

He will have completed the degree requirements for Master of Science in Anatomy and Neurobiology at Virginia Commonwealth University on the Medical College of Virginia campus, Richmond, Virginia, in August 2010. Following completion of this program, he will matriculate into the University of North Carolina School of Medicine Class of 2014.